Orbital ordering under reduced symmetry in transition metal perovskites: Oxygen vacancy in SrTiO_{3}

Chungwei Lin, Chandrima Mitra, and Alexander A. Demkov

Phys. Rev. B **86**, 161102 — Published 2 October 2012

DOI: 10.1103/PhysRevB.86.161102

Orbital ordering under reduced symmetry in transition metal perovskites: oxygen vacancy in $SrTiO_3$

Chungwei Lin, Chandrima Mitra, and Alexander A. Demkov*
Department of Physics, University of Texas at Austin
(Dated: September 19, 2012)

Using a combination of density function theory and model Hamiltonian analysis, we explain the general electronic structure features induced by an oxygen vacancy (OV) in $SrTiO_3$. We show that the most important effect caused by an oxygen vacancy is the direct on-site coupling between the $3d_{3z^2-r^2}$ and $4s$, $4p$ orbitals of Ti atoms adjacent to the vacancy caused by lifting of the local cubic symmetry. This would be the case for any transition metal perovskite under symmetry-reduced environments such as an interface, surface or a defect. We find that the OV-induced localized state is highly one-dimensional and is mainly composed of Ti $3d_{3z^2-r^2}$ orbitals along the Ti-OV-Ti axis (defined as the z-axis) and Ti $4s$, $4p$ orbitals at the OV site. The oxygen vacancy does not lead to Ti t_{2g} based localized states.

PACS numbers: 31.15.A-,71.55.-i,73.20.hb

The oxygen vacancy (OV) plays an important role in perovskites[1,2]. On the one hand, the OV can lead to localized states, trapping conduction electrons and reducing the conductivity[3]. On the other hand, they can be the source of mobile carriers[4–6]. Their presence in the ferroelectric perovskite oxides may be the cause of the formation of a permanent dipole when switching the applied field that eventually leads to device breakdown[7]. Controlling the doping of OV in a perovskite solid solution can engineer the gap size which is of fundamental importance for solar catalysts[8]. At the surface, oxygen vacancies are shown to be able to affect the patterns of the reconstructed surface and are responsible for the formation of surface states[9,10]. Even richer phenomena can happen at the interface between two perovskites[11–14]. At surfaces and interfaces, the oxygen vacancies can happen naturally, for example, to reduce the polar field[9,15], or can be induced by applying different growth conditions[5,6]. These intriguing properties of oxygen vacancies resulted in significant research interest[4–6,13,15–18].

In this paper, we combine model calculations and density functional theory (DFT) to analyze the electronic effects caused by introducing an oxygen vacancy in bulk $SrTiO_3$. The problem has been previously studied by DFT[4,17–20] but the results, including the orbital composition of the defect state, depend on the functional used and specifics of the ionic relaxation. Here, we identify the most important electronic effect in the presence of an oxygen vacancy in $SrTiO_3$ and offer a coherent picture explaining why different functionals lead to different results. We find that the most profound change caused by a vacancy is the reduction of the local cubic symmetry to C_{4v} that results in an on-site orbital coupling between the $3d_{3z^2-r^2}$ and $4s$, $4p$ orbitals of Ti atoms adjacent to the vacancy site. Furthermore, we show that this local coupling not only lowers the Ti $3d_{3z^2-r^2}$-based level below the bulk e_g conduction bands, but results in an enhanced Ti-Ti hopping across the vacancy. The latter couples orbitals of two Ti atoms adjacent to OV thus further lowering the energy of a localized level by forming a bonding state. However, OV does not significantly change the character and energy of the other four $3d$ orbitals. Therefore, t_{2g}-based localized states are not plausible. To gain further insight into the OV induced effects, we construct a tight-binding (TB) model to describe OV and

* E-mail: demkov@physics.utexas.edu

demonstrate that the local orbital mixing is indeed the most important term to reproduce DFT calculations. Our conclusions should apply to any transition metal perovskite under symmetry-reduced environments, such as a surface, an interface[21], or a point defect.

$SrTiO_3$ has a perovskite ABO_3 structure shown in Fig. 1(a). It is a band insulator with an experimental band gap of 3.2 eV[22]. The two lowest conduction bands are Ti t_{2g}^* and e_g^* bands with bandwidths of approximately 3 eV and 4 eV, respectively. The separation between these two bands, typically referred to as the crystal field splitting 10Dq and measured by the energy difference between the band centers, is estimated to be about 3 eV within the local density approximation (LDA)[18]. Interestingly, within the LDA+U (U = 8.0 eV) the splitting is reduced to about 2 eV. Once an oxygen vacancy is introduced, the local symmetry for the two Ti atoms adjacent to the vacancy site is reduced to C_{4v} [see Fig. 1 (b) and (c)]. Therefore, the original Ti e_g, t_{2g}, s and p orbitals are no longer the local eigenstates and can now couple. A C_{4v}-invariant potential has general properties $H_{C_4}(x,y,z) = H_{C_4}(-y,x,z)$ and $H_{C_4}(x,y,z) \neq H_{C_4}(x,y,-z)$. Applying first order perturbation theory where the energy shift is $\Delta E_i = \langle 3d_i|H_{c4}|3d_i\rangle$, one sees that three t_{2g} orbitals are split into a singlet xy and a doublet yz, zx whereas the e_g degeneracy is also lifted. However, since the $3d$ orbitals are quite localized, this effect may not be significant. In our DFT calculation, the t_{2g} splitting, estimated by taking the energy average, is smaller than 0.3 eV with $3d_{xy}$ higher than the other two. If estimated by the band center positions, t_{2g} orbitals split even less [see Fig. 3(d)]. From second order perturbation theory, the important orbital couplings are those between the Ti $3d$ and Ti $4s$, $4p$ orbitals as they are close in energy. Among all possible $3d$ to $4s$ and $4p$ couplings, the only two that are allowed are those between $3d_{3z^2-r^2}$ and $4p_z$, and between $3d_{3z^2-r^2}$ and $4s$. Namely, all matrix elements within $|3d\rangle$ manifold, and between $|3d\rangle$ and $|4s\rangle$, $|4p\rangle$, are zero *except* $\langle 3d_{3z^2-r^2}|H_{C_4}|4s\rangle$ and $\langle 3d_{3z^2-r^2}|H_{C_4}|4p_z\rangle$. One example, the coupling between $3d_{3z^2-r^2}$ and $4p_z$, is schematically shown in Fig. 1(c). The OV-induced C_{4v} potential changes both the energy and character of local orbitals. In terms of energy, this coupling pushes $3d_{3z^2-r^2}$ ($4s$, $4p_z$) based orbitals down (up) in energy due to the level repulsion. Unlike a static Coulomb induced energy shift, this shift is orbital dependent. All other Ti $3d$ orbitals ($3d_{3x^2-y^2}$ and three t_{2g} orbitals) remain unaffected. In terms of its orbital composition, the new $3d_{3z^2-r^2}$-based local state contains non-negligible $4s$, $4p_z$ components making it extended enough to effectively introduce hopping between the two Ti sites adjacent to the OV site. Note that direct $d-d$ hopping is negligibly small for any reasonable Ti-Ti separation[23].

Electronic structure effects caused by an OV can now be summarized as follows. It (I) adds two electrons to the lowest unoccupied levels, the Ti $3d$ levels; (II) eliminates the direct hopping between Ti and OV sites and increases the local potential at the OV site; (III) strongly lowers the energy of the Ti $3d_{3z^2-r^2}$ orbital that is adjacent to OV, while only slightly affects the energy levels of the other four $3d$ orbitals, i.e. the energy shift is orbital specific; and (IV) introduces a direct hopping between two Ti atoms across the vacancy site. One notes that effect (I) only changes the occupation and does not play any role in the single-electron picture. In other words, it has no effect until electron correlation is considered. If the effect (III) is strong such that two electrons [due to effect (I)] occupy two Ti $3d_{3z^2-r^2}$ orbitals next to OV, then the system including on-site correlation can be well described by a half-filled two-site Hubbard model, in complete analogy to the electrons at the $LaTiO_3/LaAlO_3$ interface being well described by a two-dimensional one-band Hubbard model[24].

We shall now discuss effects (III) and (IV) more quantitatively, treating the OV-induced C_4 potential as a perturbation. The OV-induced Ti-Ti hopping is parameterized by a hopping parameter $-t'$. Because the effects for $3d_{3z^2-r^2}$ to $4p_z$ and $4s$ are similar, the following discussion focuses mainly on the former. The latter case can be understood in exactly the same way. Under cubic symmetry, $3d_{3z^2-r^2}$ and $4p_z$ orbitals are the eigenstates of the local Hamiltonian and their energy difference is denoted as $\varepsilon_{4p_z} - \varepsilon_{3d_{3z^2-r^2}} = \Delta$ (with $\Delta > 0$). Writing the OV induced

couplings between $3d_{3z^2-r^2}$ and $4p_z$ at the left and right Ti sites [see Fig. 1 (b)] with respect to OV as C_- and C_+, the resulting $3d_{3z^2-r^2}$-based eigenstate becomes:

$$|a,\pm\rangle = |3d_{3z^2-r^2},\pm\rangle - \frac{C_\pm}{\Delta}|4p_z,\pm\rangle \tag{1}$$

where $\pm$ labels the Ti position relative to OV. A schematic demonstration of $|a\rangle$ is given Fig. 1 (d). Compared with the original $|3d_{3z^2-r^2}\rangle$, $|a\rangle$ becomes asymmetric with respect to z and more extended in space. The energy of $|a,\pm\rangle$ is lowered by $C_\pm^2/\Delta$ compared to that of $|3d_{3z^2-r^2},\pm\rangle$. The effective hopping Ti-Ti hopping t' is given by

$$\begin{aligned} -t' &= \langle a,-|H_{hop}|a,+\rangle \\ &\sim +\frac{C_+C_-}{\Delta^2}\langle 4p_z,-|H_{hop}|4p_z,+\rangle \end{aligned} \tag{2}$$

where H_{hop} gives the direct hopping amplitude and direct $3d-3d$ hopping is neglected. The symmetry implies that $C_+ = -C_- \equiv C$ and $\langle 4p_z,-|H_{hop}|4p_z,+\rangle = +t_p$ with t_p positive, and we get

$$-t' = -\frac{C^2}{\Delta^2}\times t_p < 0. \tag{3}$$

A similar consideration applying to $3d_{3z^2-r^2}$-$4s$ coupling leads to the same $t'>0$ conclusion (in that case, $C_+ = C_-$ but $\langle 4s,-|H_{hop}|4s,+\rangle = -t_s$ with $t_s>0$). We thus conclude that the OV induced Ti-Ti hopping is $-t'$ with $t'>0$, indicating that the bonding combination of two Ti local states ($|a,+\rangle + |a,-\rangle$) is more stable than its anti-bonding counterpart ($|a,+\rangle - |a,-\rangle$).

We can now construct a TB model to describe the OV-induced effects. The valance and conduction bands of $SrTiO_3$ can be reasonably well described in the TB approximation including only O $2p$ and Ti $3d$ orbitals with nearest neighbor hopping[22,25]. As t_{2g} orbitals preserve their character in the presence of an OV, we expect that the t_{2g} sector remains essentially unaffected. The effect that an OV removes the direct hopping between OV site and its adjacent Ti (effect II) is expected to slightly reduce the bandwidth of the t_{2g} band. Similar to the t_{2g} case, the $3d_{x^2-y^2}$ level does not change due to OV. On the other hand, the $3d_{3z^2-r^2}$ orbital is strongly perturbed due to OV-induced couplings to $4s$ and $4p_z$ states. We therefore focus on changes in the $3d_{3z^2-r^2}$-based orbital. As the $3d_{3z^2-r^2}$ orbital is highly directional, i.e. the hopping amplitude along the z direction is much stronger than those along x and y, we only consider the one-dimensional chain composed of Ti $3d_{3z^2-r^2}$ and O $2p_z$ orbitals, as illustrated in Fig. 1. The hoppings normal to the chain can be treated as a broadening source in the spectrum. We shall first write down the Hamiltonian for this 1D chain and then add the OV effect. The tight-binding Hamiltonian for the 1D chain is

$$H_{band} = \sum_i (\epsilon_d n_{d,i} + \epsilon_p n_{p,i}) + t\sum_i \left([d_i^\dagger p_i - p_i^\dagger d_{i+1}] + h.c.\right), \tag{4}$$

where $d_i^\dagger$, $p_i^\dagger$ are creation operators of Ti $3d_{3z^2-r^2}$, O $2p_z$ at unit cell i respectively. We take $\epsilon_d = 0$, $\epsilon_p = -8$ eV, $t = 3$ eV extracted from Ref.[18]. This choice of energy offset leads to a conduction bandwidth of 4 eV and a e_g-e_g^* gap of 8 eV. The *change* due to an oxygen vacancy at site 0 is

$$V_o = (\bar{\epsilon}_p - \epsilon_p)n_{p,0} + \bar{\epsilon}_d(n_{d,0}+n_{d,1}) - t\left([d_0^\dagger p_0 - p_0^\dagger d_1] + h.c.\right) - t'(d_0^\dagger d_1 + d_1^\dagger d_0). \tag{5}$$

$\bar{\epsilon}_p$ is the new energy level at OV site which should be a very large number [Effect (II)]. $\bar{\epsilon}_d(<0)$ is the energy down-shift due mainly to local Ti $|3z^2-r^2\rangle$, $|4p_z\rangle$ level repulsion [Effect (III)]. The hopping between OV site and adjacent Ti sites should vanish, which is captured by terms with coefficient $-t$ [Effect (II)]. Finally the OV-induced Ti-Ti hopping across the OV site with amplitude t' is introduced [Effect (IV)]. The total Hamiltonian with a single OV is $H_{band}+V_o$.

One should bear in mind that the d_0, d_1 in Eq. (5) are not pure Ti $3d_{3z^2-r^2}$ orbitals but have components of Ti $4p_z$ and $4s$ [$|a,\pm\rangle$ in Eq. (1)]. Values of $\bar{\epsilon}_p$ do not affect our results as long as it is a large number, and we take $\bar{\epsilon}_p = 20$ eV. To determine the values of $\bar{\epsilon}_d$ and t' requires first principle calculation. The general analysis only constrains t' to be positive. Here we choose $\bar{\epsilon}_d = -2.5$ eV and $t' = +1$ eV to be consistent with DFT results (Fig. 3(a) and Ref[18]).

Our analysis suggests that Ti $3d_{x^2-y^2}$, t_{2g} based local density of states (LDOS) is unchanged compared to the bulk counterparts, whereas the Ti $3d_{3z^2-r^2}$-based LDOS is given by the spectrum of $H_{band} + V_o$. The OV effects on the adjacent Ti sites are characterized by two parameters: $\bar{\epsilon}_d$ and t'. In order to illustrate how they influence the system, we perform an intermediate step by setting t' to zero. As discussed previously, $\bar{\epsilon}_d$ must be negative due to the level repulsion, and negative $\bar{\epsilon}_d$ implies two localized states. These two localized wave functions for $\bar{\epsilon}_d = -2.5$ eV are shown in Fig. 2(a). They can be classified by even (bonding) and odd (anti-bonding) parity due to inversion symmetry with respect to the OV site. They are degenerate with energy of 0.83 eV when $t' = 0$, and are split into 1.5 eV and -0.29 eV for bonding and anti-bonding states respectively when $t' = +1$ eV. The positive t' picks the bonding state as the ground state. The total DOS and LDOS at Ti sites adjacent to the OV are shown in Fig. 2(b). They represent the spectrum mainly derived from Ti $3d_{3z^2-r^2}$ and O $2p_z$.

To confirm that our model indeed captures the main physics of the OV, we examine several quantities from the DFT calculations for an OV is introduced in a 2x2x4 supercell. All calculations are done using the Vienna Ab-initio Simulation Package (VASP) code[26] with the plane wave cut off energy of 600 eV and with a $6\times6\times6$ Monkhorst-Pack special k-point grid[27] for integration over the Brillouin zone. The projector augmented wave pseudopotentials[28] are used. For Sr and Ti, $4s^2 4p^6 5s^2$ and $3s^2 3p^6 4s^2 3d^2$ are included, respectively. More details of the calculation can be found in Ref.[18]. The LDOS (with ionic relaxation) at the Ti site next to an OV is shown in Fig. 3(a). Here we emphasize two important aspects. First, as shown in Fig. 3(a), in the presence of an OV, the t_{2g} and $3d_{x^2-y^2}$-based DOS are quite similar to those in the bulk. The LDOS of the $3d_{3z^2-r^2}$ orbitals, however, is drastically different from its bulk counterpart. In particular, it has two peaks located at approximately 0.8 and approximately 2.6 eV [Fig. 3(a)]. According to our model, this two-peak structure corresponds to the bonding and anti-bonding localized states marked in Fig. 3(a). These two peaks should be compared with the two dashed peaks located at -1.5 and -0.29 eV shown in Fig. 2(b) from the model calculation.

Equation (1) suggests that the defect states at Ti atom adjacent to OV have appreciable $4p$ and $4s$ components. This is confirmed in Fig. 3(a) where LDOS of Ti next to OV projected on $4s$ and $4p$ orbitals are shown. The $4s$ and $4p$ components indeed have significant contributions over the energy range of these localized $3d_{3z^2-r^2}$ states [peaked around +0.8 eV and 2.6 eV (a resonance)] whereas without OV they have almost zero contribution over the same energy window (not shown). The bonding/anti-bonding character is best illustrated in Fig. 3(e) and (f) where the charge density of these two localized states (~ 0.8 eV and ~ 2.6 eV) is plotted. Their bonding (large amplitude at OV site) and antibonding (essentially zero at OV site) characters are apparent. As discussed earlier, the ~ 2eV separation between bonding and antibonding levels is too large for a direct Ti $3d-3d$ hopping, and our analysis suggests this direct hopping originates from Ti $4s$ and $4p$ components. Fig. 3(a) is also consistent with our assumption that the hopping of $3d_{3z^2-r^2}$ in the $x-y$ plane is relatively small and can be neglected when discussing localized states. We stress that the following three features – (1) two split, localized $3d_{3z^2-r^2}$ levels [Fig. 3(a)], (2) the non-zero $4s$, $4p$ contributions at these two energy levels [Fig. 3(a)], and (3) the bonding/antibonding characters displayed in the charge density plot [Fig. 3(e) and (f)] – are very robust in the DFT calculations. As shown in Fig. 3(a)-(c), using a different functional, such as LDA+U with U=8.0 eV [Fig. 3(b)], or not relaxing the ionic positions [Fig. 3(c)] cannot eliminate them[18]. All three features are derived from the OV-induced local couplings and are well captured in our simple one-dimensional model [Eqs. (4) and (5)].

To summarize, we identify that the most important electronic effect introduced by an oxygen vacancy is the local orbital coupling between the $3d_{3z^2-r^2}$ and $4s$, $4p$ orbitals at the two adjacent Ti sites. All other Ti $3d$ orbitals, t_{2g} and $3d_{x^2-y^2}$, are essentially unaffected and their spectral features are similar to those without a vacancy. For the two Ti sites adjacent to OV, the OV-induced orbital couplings push the $3d_{3z^2-r^2}$ based orbitals down in energy, and lead to one localized state at each Ti site. The admixture of local $4s$, $4p$ components introduces a direct Ti-Ti hopping across the vacancy that couples these two localized states and pushes their bonding combination further down in energy. The polaronic effects (lattice relaxation)[29] are relatively minor. The salient feature of the localized state is that it is highly one-dimensional. Experimentally, this implies that in the presence of an oxygen vacancy in $SrTiO_3$, a probe including $4s$ and $4p$ orbitals as final states such as x-ray adsorption spectroscopy (Ti M or L_1-edge, for example) should see these peaks near the Ti $3d$ bands and well below the $4s$-$4p$ empty bands. The intensity of these peaks can be used to characterize the vacancy concentration. We emphasize that this behavior is general for all transition metal perovskites and that only one of the e_g ($3d_{3z^2-r^2}$ taking the z axis along the Ti-OV-Ti line) levels is lowered due to an adjacent vacancy. Moreover, we suggest that in general under symmetry-reduced environments, such as a surface, an interface or a nearby defect, the corresponding change of the local orbital character is the most important electronic effect, and should be the first mechanism to include in any model study. In addition to the original transition metal $3d$ component, the resulting local orbitals would typically involve more extended $4s$, $4p$ components, therefore the dangling bonds (localized and partially filled states) can be spatially much larger than expected solely on the $3d$-orbital basis[30]. It is this extended character of the local state that is responsible for the hybridization of sites adjacent to a vacancy.

Answering whether the localized e_g state has an energy lower than the bottom of the t_{2g} band and becomes a true bound state requires an accurate DFT calculation and results may indeed vary depending on the functional used, as shown in Fig. 3(a) and (b). Since the OV mainly lowers one of the Ti e_g levels, the crucial factor in forming the bound state is the crystal field e_g-t_{2g} splitting in the bulk system. The general trend is that within the LDA, the crystal field is large (10Dq is roughly 3 eV) and the localized level is a band resonance close to (~ 0.2 eV) the bottom of the t_{2g} bands[17,18]. When using the Hubbard U correction (LDA+U) on Ti sites or applying the hybrid functional[31] to correct the bandgap of $SrTiO_3$, the crystal field splitting decreases (10Dq is roughly 2 eV) and the e_g localized state becomes a true bound state[17,18]. If an OV-induced bound state does form, it traps two electrons at two Ti sites adjacent to OV, and can be regarded as a charge (2^-) entity that can move under an external electric field[7,32].

We thank Agham Posadas and Hosung Seo for insightful discussions and critical reading of the manuscript. This work is supported by the U.S. Department of Energy (DOE) under Grant No. DESC0001878 and all calculations are done at the Texas Advanced Computing Center.

[1] J. N. Eckstein, Nature Mater. **6**, 473 (2007).

[2] D. Kan, T. Terashima, R. Kanda, A. Masuno, K. Tanaka, S. Chu, H. Kan, A. Ishizumi, Y. Kanemitsu, Y. Shimakawa, et al., Nature Mater. **4**, 816 (2005).

[3] H. C. Nguyen and J. B. Goodenough, Phys. Rev. B **52**, 8776 (1995).

[4] W. Luo, W. Duan, S. G. Louie, and M. L. Cohen, Phys. Rev. B **70**, 214109 (2004).

[5] W. Siemons, G. Koster, H. Yamamoto, W. A. Harrison, G. Lucovsky, T. H. Geballe, D. H. A. Blank, and M. R. Beasley, Phys. Rev. Lett. **98**, 196802 (2007).

[6] A. Kalabukhov, R. Gunnarsson, J. Börjesson, E. Olsson, T. Claeson, and D. Winkler, Phys. Rev. B **75**, 121404 (2007).

[7] C. H. Park and D. J. Chadi, Phys. Rev. B **57**, R13961 (1998).

[8] T. Qi, M. T. Curnan, S. Kim, J. W. Bennett, I. Grinberg, and A. M. Rappe, Phys. Rev. B **84**, 245206 (2011).

[9] H. Seo and A. A. Demkov, Phys. Rev. B **84**, 045440 (2011).

[10] S. Kimura, J. Yamauchi, M. Tsukada, and S. Watanabe, Phys. Rev. B **51**, 11049 (1995).

[11] A. Ohtomo, D. A. Muller, J. L. Grazul, and H. Y. Hwang, Nature **419**, 378 (2002).

[12] S. Okamoto and A. J. Millis, Nature **428**, 630 (2004).

[13] A. Ohtomo and H. Y. Hwang, Nature **427**, 423 (2004).

[14] S. Thiel, G. Hammerl, A. Schmehl, C. W. Schneider, and J. Mannhart, Science **313**, 1942 (2006).

[15] N. Nakagawa, H. Y. Hwang, and D. A. Muller, Nat. Mater. **5**, 204 (2006).

[16] A. S. Kalabukhov, Y. A. Boikov, I. T. Serenkov, V. I. Sakharov, V. N. Popok, R. Gunnarsson, J. Börjesson, N. Ljustina, E. Olsson, D. Winkler, et al., Phys. Rev. Lett. **103**, 146101 (2009).

[17] D. Ricci, G. Bano, G. Pacchioni, and F. Illas, Phys. Rev. B **68**, 224105 (2003).

[18] C. Mitra, C. Lin, J. Robertson, and A. A. Demkov (2011), (submitted).

[19] J. P. Buban, H. Iddir, and S. Öğüt, Phys. Rev. B **69**, 180102 (2004).

[20] J. Carrasco, F. Illas, N. Lopez, E. A. Kotomin, Y. F. Zhukovskii, R. A. Evarestov, Y. A. Mastrikov, S. Piskunov, and J. Maier, Phys. Rev. B **73**, 064106 (2006).

[21] J. Lee, C. Lin, and A. A. Demkov (2012), (submitted).

[22] K. van Benthema, C. Elsasser, and R. H. French, J. Appl. Phys. **90**, 6156 (2001).

[23] Using the Harrison's rule for Ti atom with a Ti-Ti separation of 3.8Å[18], the hopping amplitude is estimated to be ~ 0.1 eV.

[24] S. S. A. Seo, M. J. Han, G. W. J. Hassink, W. S. Choi, S. J. Moon, J. S. Kim, T. Susaki, Y. S. Lee, J. Yu, C. Bernhard, et al., Phys. Rev. Lett. **104**, 036401 (2010).

[25] S. Okamoto, A. J. Millis, and N. A. Spaldin, Phys. Rev. Lett. **97**, 056802 (2006).

[26] G. Kresse and J. Furthmüller, Phys. Rev. B **54**, 11169 (1996).

[27] H. J. Monkhorst and J. D. Pack, Phys. Rev. B **13**, 5188 (1976).

[28] P. E. Blöchl, Phys. Rev. B **50**, 17953 (1994).

[29] M. O. Selme and P. Pecheur, J. Phys. C. **16**, 2559 (1983).

[30] U. Diebold, J. F. Anderson, K.-O. Ng, and D. Vanderbilt, Phys. Rev. Lett. **77**, 1322 (1996).

[31] J. Heyd, G. Scuseria, and M. Ernzerhof, J. Chem. Phys. **118** (2003).

[32] R. Meyer, R. Liedtke, and R. Waser, Appl. Phys. Lett. **86**, 112904 (2005).

Figure captions

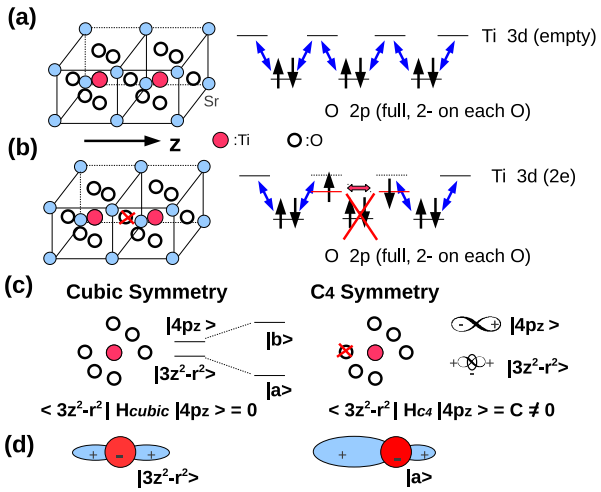

FIG. 1: (Color online) Bulk structure and effects due to one oxygen vacancy. (a) Clean bulk system. All oxygen $2p$ orbitals are occupied and all Ti $3d$ orbitals are empty leading to a band insulator. (b) With an oxygen vacancy (OV) is presented, the local level at OV site becomes very large, the Ti $3d$ levels next to OV is lowered. Blue double arrows represent the direct Ti $3d$- O $2p$ hoppings. We define the Ti-OV-Ti axis as z throughout our discussion. (c) Effects of local orbital character on Ti next to OV. (Left) Under the cubic symmetry, $3d_{3z^2-r^2}$ and $4p_z$ orbitals are local eigenstates. The coupling between $3d_{3z^2-r^2}$ and $4p_z$, induced by C_4 symmetry, changes character of the local eigenstates, pushing $3d_{3z^2-r^2}$-based ($|a\rangle$) and $4p_z$-based ($|b\rangle$) orbitals down and up in energy respectively. (d) The schematic $3d_{3z^2-r^2}$-based orbitals under cubic and C_4 symmetry. Under cubic symmetry, $3d_{3z^2-r^2}$ is an eigenstate while under the reduced C_4 symmetry, it mixes significantly with $4p_z$ state making the resulting $|a\rangle$ asymmetric and more extended.

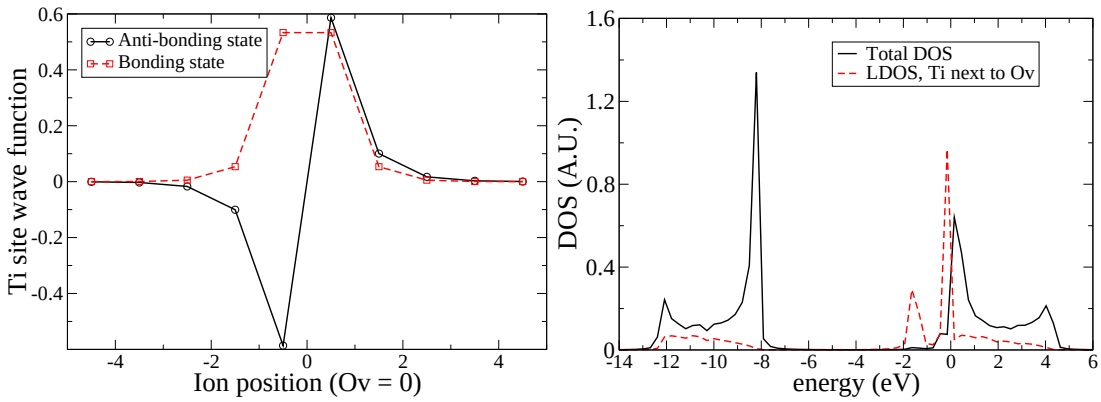

(a) (b)

FIG. 2: (Color online) (a) Wave functions of two localized states projected at Ti sites. 0 is the position of oxygen vacancy, integers label O positions, and half integers Ti positions. They are almost degenerate when $t' = 0$ and are split to bonding and antibonding states when $t' \neq 0$. (b) Total DOS with an OV and LDOS of Ti next to the OV. Here $\bar{\epsilon}_d = -2.5$ eV and $t' = 1$ eV are used. The integrated total DOS (black, solid) is normalized to 2, whereas the integrated LDOS (red, dashed) 1. The contributions of total DOS below -8 eV are mainly from O $2p$, while those above 0 eV Ti $3d$. A broadening of 0.05 eV is used.

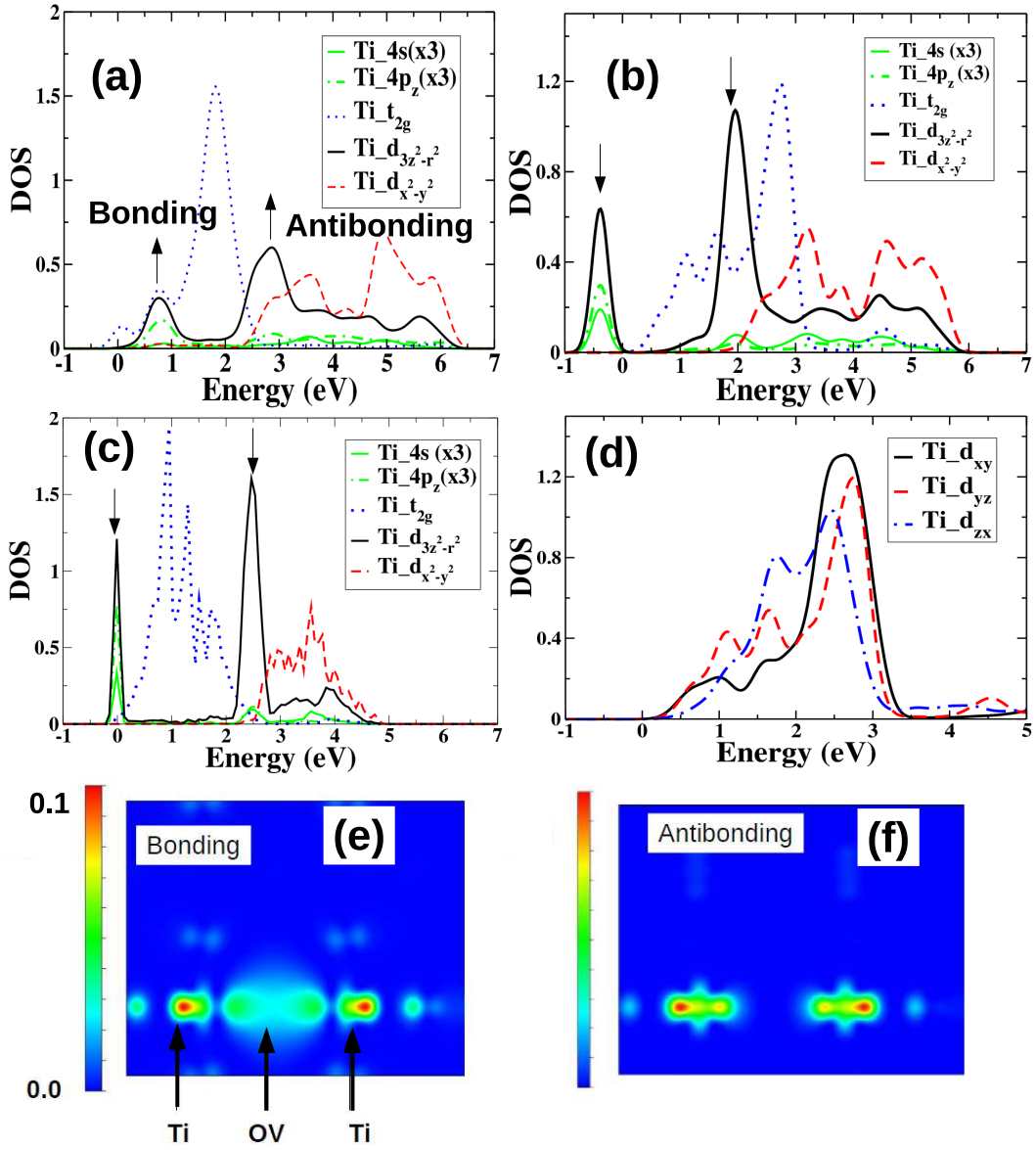

FIG. 3: (Color online) (a) LDOS of Ti next to the OV computed by DFT (without U)[18]. The $3d_{3z^2-r^2}$ peaks at ~ 0.8 and ~ 2.6 eV are interpreted as bonding and antibonding localized states. (b) Same Ti LDOS computed by LDA+U with U=8.0 eV with ionic relaxation. (c) Same Ti LDOS computed by LDA without ionic relaxation. Only one of three t_{2g} orbitals is shown since they are close in energy. In all three cases, the $3d_{3z^2-r^2}$ bonding/anti-bonding peaks (indicated by arrows) are associated with substantial Ti $4s$ and $4p$ contributions. Note the $4s$ and $4p$ components are multiplied by 3 for clarity. (d) Three t_{2g} orbitals LDOS computed by LDA+U with U=8.0 eV with ionic relaxation. The splitting, estimated by taking the energy average, is smaller than 0.3 eV with $3d_{xy}$ higher than the other two. Similar small t_{2g} splitting is observed in the LDA calculations. (e) The charge density plot at ~ 0.8 eV in (a). At the OV site the charge density is extended enough to cover the whole OV site, which a character of the bonding state. (f) The charge density plot at ~ 2.6 eV in (a). At the OV site the charge density is almost zero but is extended to the neighboring Ti sites, which is a character of the antibonding state.